Laser assisted chemically shaped unstable resonator, for high power coherent laser diodes

Salvador Guel-Sandoval
Instituto de Investigacion en Comunicacion Optica, Universidad Autónoma de San Luis Potosi
Alvaro Obregon 64, 78000 San Luis Potosi, S.L.P., Mexico

Alan H. Paxton and Stephen D. Hersee
Center for High Technology Materials, University of New Mexico
Albuquerque NM, 87131-6081, USA

John G. McInerney
Department of Physics, University College Cork, Ireland

Recibido el 13 de junio de 1998; aceptado el 3 de noviembre de 1998

Laser assisted chemical etching (LACE) is used to etch a continuous graded channel, set inside a wide stripe graded-index and separate-confinement heterostructure (GRIN-SCH) for laser diodes, grown by metal organic chemical vapor deposition (MOCVD). After a procedure of growing-etching-regrowing, a two-part waveguide is formed inside such modified structure, that is characterized by a negative change in the lateral effective refractive index (ERI). This effects the cavity to work as an unstable resonator. Procedures on the photoetching process are described, including the GaAs photochemistry and the optical system, with special emphasis on the fabrication of the approximately parabolic channels, as this represents a novel step. We call the cavity fabricated by this method, the shaped unstable resonator (SHUR).

Keywords: Semiconductor lasers; high power; spatial coherence; unstable resonators; laser assisted chemical etching (LACE)

Se usa una técnica conocida como ataque químico inducido por láser (AQIL) para fabricar un canal graduado continuo, que se coloca dentro de una heteroestructura de confinamiento separado con índice graduado (HCS-INGRA), crecida por deposición química de compuestos metalorgánicos en fase de vapor (DQCMV). Después de un proceso de crecimiento-ataque-recrecimiento, queda conformada dentro de la estructura, una guía de onda doble que se caracteriza por tener un índice efectivo de refracción (IER) que varía negativamente en la dirección lateral. Esto hace que la cavidad trabaje como un resonador inestable. En el trabajo se describen tanto el proceso del fotoataque y la fotoquímica del GaAs, así como el sistema óptico usado, con especial énfasis en la fabricación de los canales aproximadamente parabólicos, ya que éste es un proceso nuevo. De acuerdo con el método usado para fabricarlo, este nuevo resonador se designó como resonador inestable figurado (REIF).

Descriptores: Láseres semiconductores; alta potencia; coherencia espacial; ataque químico inducido por láser (AQIL)

PACS: 42.55.Px; 42.60.Da; 82.65.Yh

1. Introduction

Laser assisted chemical processing (LACP) is the generic name for a relatively new technique that has become an important branch of the materials processing. It combines a variety of disciplines, including: optics, chemistry, semiconductor physics and materials science, among others. The technique uses a beam of monochromatic photons (laser) to control reactive processing near solid surfaces. The processing actions can be material deposition (writing), solid doping, alloying or etching.

The reactions that effect the processing (deposition or etching) can be initiated by purely photochemical events such as direct dissociation of molecules by photons (photolytic), or the reactions can result from heating due to absorption of the laser beam in a gas or solid at a gas-solid interface (pyrolytic.) Alternatively chemical reactions can be driven by photogenerated electron-hole pairs formed near the surface of the substrate on which the reactions occur [1].

The essential components in any LACP experiment are nearly the same: a cell that encloses the solid substrate with the gaseous or liquid reagents, an optical system and a laser. The laser beam can be directed either parallel to the substrate or perpendicular to it. Laser wavelengths range from the infrared to the ultraviolet and the beam can be pulsed or continuous.

The choice of some particular conditions (laser beam direction, wavelength etc.) depends basically on the type of process and the materials involved. For example for the photoetching of a semiconductor it is important the energy of the photon to be equal or larger than the band-gap of the substrate to guaranty proper light absorption. Also in this case, the laser beam is mostly perpendicularly directed to the sample.

In a semiconductor (GaAs for instance) the purely etching process is known as laser assisted chemical etching (LACE) process. In this case reactions derive from photogenerated

electron-hole pairs when laser light is absorbed by the material, in presence of an etching solution or gas. (See Appendix A.)

LACP is therefore an alternative choice to traditional etching and deposition, and is a new tool that can be exploited in the processing of a diversity of materials for optoelectronic and integrated optic devices fabrication. So far, LACP has been used successfully applied in semiconductors, metals and polymers [2, 3]. Several advantages offered by this LACP technique are: low temperature processing, maskless patterning and beam controlled anisotropy.

The purpose of this work is to describe the experimental procedure that availed to configurate a new type of unstable resonator for high power coherent semiconductor laser diodes, where LACE was used. The procedure, which will be explained in detail later, consists basically in integrating by means of a growth-LACE-regrowth sequence, a two part antiguide inside a diode laser grade index and separated confinement heterostructure (GRIN-SCH) with a GaAs substrate and $Al_xGa_{1-x}As$ cladding regions ($GaAs/Al_xGa_{1-x}As$), grown by MOCVD.

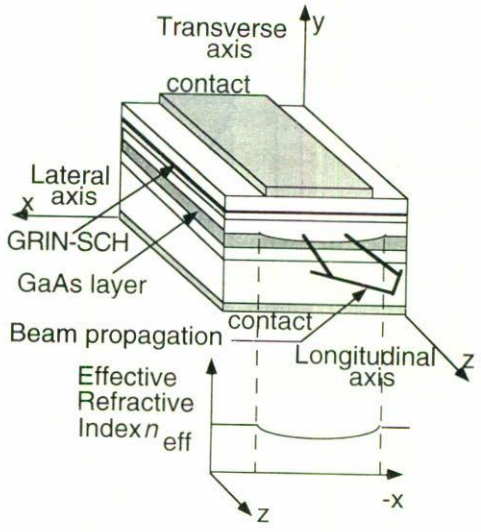

FIGURE 1. Schematic representation illustrating the SHUR laser concept. The curve area represents the photoetched GaAs layer (secondary wavegide) on top of which an $Al_xGa_{1-x}As$ layer is regrown and then the GRIN-SCH (primary wavegide) is completed. The medium becomes an unestable resonator after this operation due to the negative lateral effective index variation. The detail GRIN-SCH structure is show in Sect. 2, and the fabrication procces in discussed in Sect. 3.

2. Survey to unstable resonator laser diodes

Because of their capacity to deal with large lasing volumes and to eliminate high order lateral modes, unstable resonators (URs) [4–6] have become an important approach in the development of high power coherent laser diode technology, simultaneously with array systems [7–10], Talbot effect designs [11–13] and more recent the master oscillator power amplificator (MOPA) configurations [14, 15].

Several UR cavity configurations are possible in a semiconductor laser. In 1980, Bogatov *et al.*, built an asymmetrical UR laser diode by grinding and polishing a cleaved facet into the shape of a curved surface, using diamond paste and a nylon string [16]. Subsequently in 1985 Craig *et al.* [17] and Salzman *et al.* [18], reported fabrication of similar UR diode lasers using wet chemical etching and reactive-ion-etching (RIE) techniques, respectively. This early works demonstrated the effectiveness of the UR method by showing stable far field intensity distributions.

Later works by Largent *et al.* [19], Tilton *et al.* [20] and more recently DeFreez *et al.* [21], have shown the soundness of this approach by using improved techniques. The first group used reactive ion etching (RIE) to anisotropically etch a curved facet at one end of the laser cavity. The second and third groups reported fabrication of a similar UR laser but using instead an even more controllable focused-ion-beam micromachining (FIBM) technique to implement the curved facet mirror.

A different approach, that it is believed will lead to a more manufacturable device, consists in integrating the diverging elements inside the cavity by using a two part waveguide. The first waveguide is an asymmetric GRIN-SCH with the quantum well gain region. The lasing mode also couples to a secondary waveguide located beneath or above the primary waveguide, and in which diverging elements are incorporated to provide the unstable resonator action.

One example of this is the regrown lens train (RLT) laser [22], were negative diverging lens elements are etched into a GaAs layer, above the GRIN-SCH, and subsequently regrowth with a lower index p-type cladding layer.

The (SHUR) laser [23] (shown schematically in Fig. 1), that also uses a two part waveguide; is another approach to achieve high power with high coherence. The SHUR laser is in some respects similar to the RLT laser, however the diverging elements are incorporated in some different manner. The first waveguide is the main GRIN-SCH region. The secondary waveguide is a GaAs ($n = 3.59$) layer below the main region, that has been previously photoetched with the aid of an almost parabolic laser beam, and embedded between a lower index $Al_xGa_{1-x}As$ ($x = 0.4$, $n = 3.324$) material. This non-planar guide causes the effective refractive index (ERI) of the medium to vary almost linearly with the thickness of the GaAs layer in the lateral direction, being higher towards the sides of the device, as shown in the lower part of Fig. 1. In this way the optical cavity becomes an unstable resonator. Such thus modified structure, fulfills the requirements of a theoretical model that predicts single mode operation in a semiconductor laser, as long as radiation takes place in a medium with diverging index profile with a negative quadratic variation in the lateral direction [24].

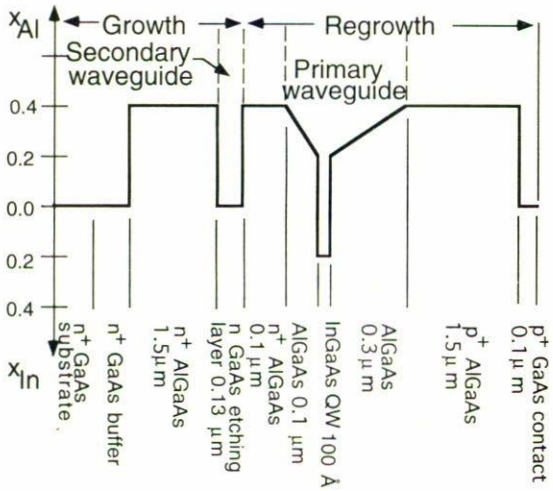

FIGURE 2. Transverse schematic view, not to scale, of the GRIN-SCH for SHUR laser showing the variation of the composition. The structure is grown up to the GaAs layer and etched, then it is regrown until completed.

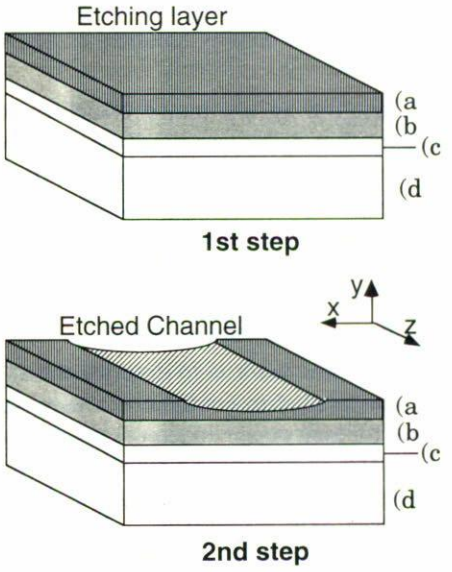

FIGURE 3. Schematic view (not to scale) of the grown structure, before (1 st step) and after (2nd step) laser assisted chemical etching (LACE) has been performed to photoetch channels along the wafer. After 2nd step, the wafer is returned back to the MOCVD reactor to be regrowed. Only an individual device is shown. The layers specifications in both structures are as follows: a) 0.13 μm n-GaAs, b) 1.5 μm n^+-$Al_{0.4}Ga_{0.6}As$, c) n^+-GaAs buffer layer, d) n^+-GaAs substrate.

3. SHUR fabrication steps

The key issue in this paper is to describe in detail the SHUR fabrication. This takes place in three steps. It starts by growing the GRIN-SCH structure shown in Fig. 2. Beginning with a n^+-type GaAs substrate, a n^+-GaAs buffer is grown followed by a 1.5 μm n^+-type cladding $Al_{0.4}Ga_{0.6}As$, on top of which an n-type GaAs layer of 0.13 μm is deposited, as shown in Fig. 3 (1st step). At this point the growth is interrupted.

In the second step the wafer is removed from the MOCVD reactor and linear arrays of parabolic channels are photoetched into the upper n-type GaAs layer. Fig. 3 (2nd step) is an schematic illustration of one individual device showing the structure after this is done. These channels are etched by using the central lobe of a far field slit diffraction pattern (*i.e.*, the Fourier transform) [25], that is focused onto the sample, while the sample is immersed in an aqueous etching solution. (The optical system used is described in Appendix B.) By using a stepper, many channels can be produced on the sample by multiple exposures.

To complete the epitaxial structure (3rd step), the wafer was returned to the MOCVD reactor, and the upper layers were grown, as seen in Fig. 4. This was done by regrowing a 0.1 μm $n^+Al_{0.4}Ga_{0.6}As$ cladding on top of the etched GaAs layer, followed by a 0.1 μm undoped $Al_xGa_{1-x}As$ (x =0.4–0.2) grading, and then a 100 Å $In_{0.2}Ga_{0.8}As$ active layer. Subsequent regrowth steps on the p-side were first a 0.3 μm undoped graded $Al_xGa_{1-x}As$ (x =0.2–0.4) after the active layer, then a 1.5 μm p^+-type $Al_{0.4}Ga_{0.6}As$ cladding, and finally a p^+-GaAs contact 0.1 μm cap layer. Substrates were n-type Si doped GaAs wafers, with a doping concentration of about 2×10^{18} cm^{-3}, and orientation (100). The thickness was 18.5 ± 0.5 mil and the diameter two inches. Tellurium

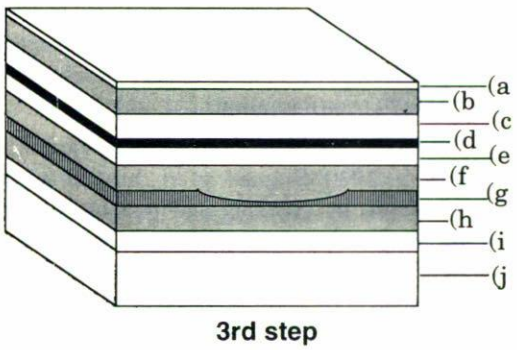

FIGURE 4. Schematic view not to scale of the finished structure. After regrowth (3rd step) the approximately parabolic etched profiles can act like negative lenses and can deviate the high order lateral modes more than the low. The layers specifications are as follows: a) 0.1 μm p^+-GaAs contact, b) 1.5 μm p^+-$Al_{0.4}Ga_{0.6}As$, c) 0.3 μm $Al_xGa_{1-x}As$ (x = 0.4–0.2), d) 100 Å $In_{0.2}Ga_{0.8}As$, e) 0.1 μm $Al_xGa_{1-x}As$ (x = 0.2–0.4), f) 0.1 μm n^+-$Al_{0.4}Ga_{0.6}As$, g) 0.13 μm n-GaAs, h) 1.5 μm n^+-$Al_{0.4}Ga_{0.6}As$, i) n^+-GaAs buffer layer, j) n^+-GaAs substrate.

was used as the n-type dopant (1×10^{18} cm^{-3} for the buffer and cladding layers, and 5×10^{16} cm^{-3} for the etching layer); while Carbon and Zinc were used for the p-side, (1×10^{18} cm^{-3} for the cladding and 1×10^{19} cm^{-3} for cap layers respectively.)

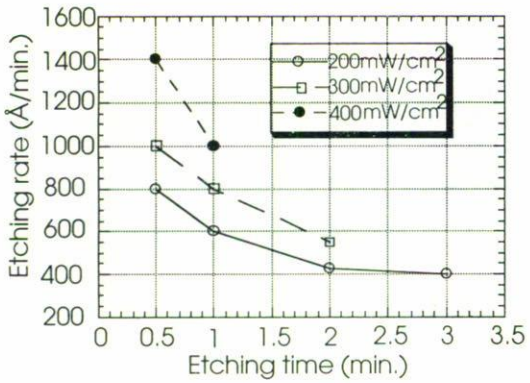

FIGURE 5. Graph showing the variation of etching rate *versus* etching time for same range of intensities and times as in previous figure. As one could expect, for small times, etching rate is larger since the etching process is surface reaction limited and the oxide is removed almost as fast as it is formed. For longer times the oxide begins to passivate the GaAs surface and slow the etching.

3.1. LACE analysis and results

The laser etching process was examined at different power levels in order to elucidate the controlling etching parameters. Laser output power was ranged between 0.05 to 10 W (λ = 488 nm) corresponding to power densities of $\sim 1.5 \times 10^2$ and $\sim 3 \times 10^4$ mW/cm^2 respectively, at the etching plane. Etching times were set between 0.5 to 5.0 minutes. Optimum channel characteristics resulted for a range of laser power among 0.05 W ($\sim 1.5 \times 10^2$ mW/cm^2) and 1 W ($\sim 3 \times 10^3$ mW/cm^2) and for etching times ranging between 0.5 and 4 minutes.

Figure 5 shows the variation of the etching rate as function of the etching time for etching intensities of 200, 300, and 400 mW/cm^2, respectively. As would be expected it is observed the same effect characteristic in any wet chemical etching experiment. For small times (< 0.5 min.) the etching rate is higher than for larger times (> 0.5 min.) since when etching starts no oxide is formed yet and the only etching limiting factor is the speed at which the reaction between the substrate surface and the reagents takes place (surface reaction controlled process.) As the etching time becomes larger, the reaction becomes limited by the oxide formation on the substrate and the reaction rate diminishes (similar to a diffusion controlled process.)

At higher power levels (5–10 W) etching presented some difficulties, resulting in delineated channels that some times showed many pits. Those pits were more evident in some samples than others, presumably due to defects and/or to unsuitable cleaning conditions. At even higher laser powers (> 10 W) some samples showed no etching at all. Even though such effect is not well understood, is supposed that at very high power levels the sample heating is sufficiently great that local vaporization of the solution results, however no bubbles were observed in the etch solution [26]. Other probable explanation could be that at high power the electron-hole pair production is high enough to favor a thick oxide formation that inhibits the etching, since the oxide is not removed as fast as it is formed.

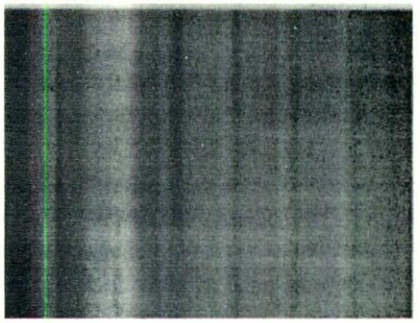

FIGURE 6. Photoetched channels. Intensity 300 nW/cm^2, etch time 2 min. Channels separation is 400 μm and channels width is 160 μm.

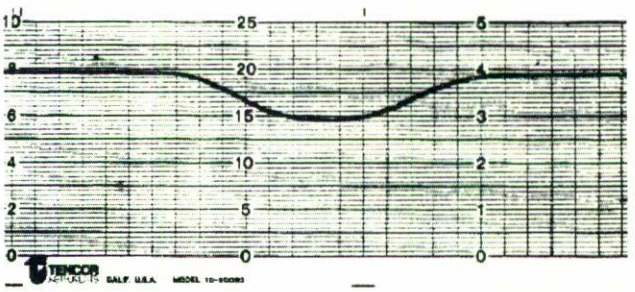

FIGURE 7. Alpha-step profiles of channels etched at and etching intensity of 300 mW/cm^2 and etching time of 2 min. Full scale in vertical direction is 5000 Å. Scale in horizontal direction is 10 μm/division, each division equals 5 mm.

Nevertheless, some authors seem to have used up to 8 W of power at 514 nm with good results [27]. Another inconvenience of using high level powers (> 10 W), is the damage that this can cause to some of the optical components in the etching system. These effects made difficult to characterize the etching at such high power levels.

All the intensities were measured by setting down a power meter at the etching plane and then dividing the power by the approximate beam area. Although if absorption and reflectance of the etching solution are taken in account, the effective etching intensities are smaller than these directly measured. Such values were not determined in the present work; however, to discount always the same amount of absorbed and reflected intensities, the concentration of the etching solution and its height above the substrate were kept constant during all etching sessions.

Figure 6 is a Nomarski photograph of typical etched channels for an etching intensity of approximately 300 mW/cm^2 and etching time of 2 minutes using a slit B width of $\sim$ 200 μm (see Fig. 9) that resulted in an etched width of $\sim$ 160 μm. Measurements of the channel profiles to determine the etch depth and etch rate, were done by using an Alpha-step profilometer whose smallest scale allowed measurement down to 50 Å. An etched continuous smooth

channel profile is shown in Fig. 7; scale in horizontal direction is 10 μm per 5 mm while full scale in vertical direction is 5000 Å. When those profiles were analyzed, it was found the etching fitted to a parabolic shape up to $\sim$ 50%, suitable for a SHUR design.

The most important issue concerning photoetching process was about overetching the GaAs layer. Emphasis on this point was done since overetching is disastrous to the process as it could destroy the active layer in the GRIN-SCH and the SHUR laser would not be possible under these circumstances. So in order to determine a safe range of exposures, the etched depth variation at the top end, center and bottom end of a centimeter long sample with several etched channels, was settled. This was done by calculating the average value of the etch depth at those regions. Etchings were performed at 300 mW/cm^2 of light intensity and 1 minute of etching time.

From this procedure, a maximum probable variation of 300 Å could be noted. Then to provide enough margin to protect the substrate from any possible overetching, a safety range of 300 Å to the desired etching, was assigned. So for a maximum desired etched depth fixed in 1000 Å (0.1μm) the GaAs etching layer should have a thickness of 1300 Å (0.13 μm.) For a such etching value and a channel width of 160 μm, a magnification $M = 7.721$ was obtained in agreement to model [28]. These results, however, become an inconvenience since a variation in the etch depth introduces a variation in the value of M (this alters the laser characteristics.) For example, if the etch depth varies 300 Å the value of M varies $\sim$ 20% when the etched depth is 160 μm.

Etching experiments were performed using (100) oriented GaAs, but there wa s not any significant difference by etching the channels perpendicular to the [110] or the [1$\bar{1}$0] direction. In the first case the more reactive (111)B plane (As atoms with two unsaturated bonds per atom) is exposed to the reactive aqueous solution. In the second, the less reactive plane (111)A (Ga atoms) is exposed [29]. All photoetching experiments were performed at room temperature.

It was observed that etching was very sensitive to defocusing of the optical system and special precautions were required to carefully control the laser beam profile. Oscillation of the Ar^+ laser in the TEM_{00} was also necessary. Also channels etched on sections of the wafer whose morphology showed a lack of uniformity revealed deep pits formed during the etching. This was probably due to some kind of crystal non-uniformities or surface contamination that enhanced the etching.

4. Fabrication of SHUR laser devices

The SHUR laser fabrication was performed following a typical clean room wide stripe laser processing. In Fig. 8, a transverse schematic view (not to scale) of the finished device is shown. Stripe masks having a 400 μm period were used with positive resist to define the metal (p-side) contact side. Two stripe contact widths were used during the processing, 80 and 140 μm. Three different etching channel depths 800,

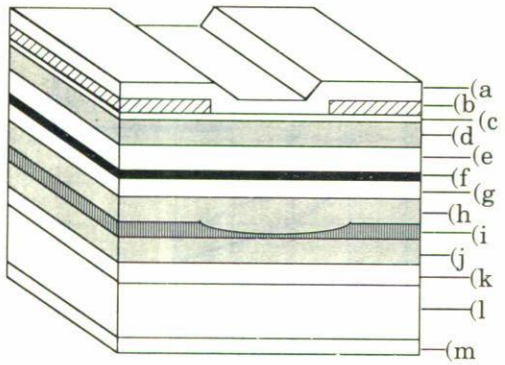

FIGURE 8. Finished SHUR laser device. The layers specifications are as follows: a) 300 Å/300 Å/3000 Å: Ti/Pt/Au, b) 900 Å Si_3N_4, c) 0.1 μm p^+-GaAs contact, d) 1.5 μm p^+-$Al_{0.4}Ga_{0.6}As$, e) 0.3 μm $Al_xGa_{1-x}As$ (x = 0.4–0.2), f) 100 Å $In_{0.2}Ga_{0.8}As$, g) 0.1 μm $Al_xGa_{1-x}As$ (x = 0.2–0.4), h) 0.1 μm n^+-$Al_{0.4}Ga_{0.6}As$, i) 0.13 μm n-GaAs, j)1.5 μm n^+-$Al_{0.4}Ga_{0.6}As$, k) n^+-GaAs buffer layer, l) n^+-GaAs substrate, m) 300 Å/300 Å/3000 Å: AuGe/Ni/Au.

500 and 300 Å were used while the channel width was kept constant and approximately equal to 160 μm. The cleaved cavity length of the devices was fixed at 500 μm.

Performance of SHUR lasers were described in more detail in Ref. 23. However for the sake of comparison with other similar devices, some of the achieved data will be mentioned here: up to 770 mW (47% in main lobe) pulsed, per facet, were obtained within a far field lobe of 2 times the difraction limit (DL) at full width of half maximum (FWHM) with an external quantum efficiency of 66% double facet. This was for a threshold current of 1.4 A.

5. Conclusions

The experimental results indicated that the etching method was adequate for producing satisfactory feasibility results. There are, however, some differences between the desired etching profile and the real one produced by this technique that should be taken into consideration for future modeling improvement.

A careful analysis of channels with similar etching characteristics showed that the profile in Fig. 7 matched up to an inverted sinc^2 function rather than a parabola, as expected, since the etching beam (Appendix B) resembles such a shape. The deviation between such two functions being more notorious at the edges of the channel and surely accentuated by the almost linear dependence of the etched depth on light intensity. Measurements indicated that only approximately 50% of the etched width fitted to the desired parabolic profile; which limited the maximum useful size of the laser contact to be approximately the half the width of the etching, since the remaining non-parabolic region would introduce non-linearities (although the whole channeled structure still maintained its condition of antiguide.)

Furthermore a key characteristic of the SHUR cavity is that gain discrimination depends almost exclusively on geometric factors that are determined by etching conditions and are in principle flexible yet easily manageable; this allows to select some required value of divergence. Besides, in spite of the similarity between the RLT and the SHUR cavities, there are nevertheless some differences since the SHUR laser cavity contains none of the scattering interfaces that are present at each of the "lens" elements in the RLT cavity.

Acknowledgments

Part of this work was performed while the first author was at the CHTM of the UNM. It was partially supported by the USAF Phillips Laboratory and by the Consejo Nacional de Ciencia y Tecnologia, (CONACyT), Mexico. The authors, also appreciate the support of the Crystal Growth facility personnel at the CHTM, for growing the samples.

Appendix A. Laser assisted chemical etching of GaAs

The integration on-the-chip of the parabolic etched channels is fundamental to the concept of the SHUR cavity. The successful performance of the process depends on how effectively the etching parameters can be controlled. This requires a reasonable understanding of the reactions that take place during the photoetching procedure as well as a description of the optical system used. These topics will be treated in this and the next paragraphs.

It is an accepted theory in all reported experiments of GaAs photochemical etching, that the etching process is assisted by the production of the photogenerated excess of minority carriers [30]. As consequence of the built-in electric field, caused by the band bending, photogenerated holes or electrons migrate towards the surface of the substrate where they favor oxide formation [31].

Holes have been supposed to assist in the photochemical etching of n-type GaAs by oxidative decomposition. Oxidation and then dissolution of resultant products are usually carried out simultaneously by a mixture of reagents in a same solution or gas where the sample is immersed.

The GaAs decomposition by oxidation is thought to be due to the following surface reaction [32]:

$$\mathrm{GaAs} + 6\mathrm{h}^{+} \rightarrow \mathrm{Ga}^{3+} + \mathrm{As}^{+3}, \tag{1}$$

where the ionic states for gallium and arsenic are Ga^{3+} and As^{3+}.

The separate reactions for the gallium in presence of water are as follows:

$$\begin{aligned} 3\mathrm{H_2O} &\Leftrightarrow 3\mathrm{H}^{+} + 3(\mathrm{OH})^{-}, \\ \mathrm{Ga}^{3+} + 3(\mathrm{OH})^{-} &\rightarrow \mathrm{Ga(OH)_3}, \\ 2\mathrm{Ga(OH)_3} &\rightarrow \mathrm{Ga_2O_3} + 3\mathrm{H_2O}. \end{aligned} \tag{2}$$

While reactions for arsenic are

$$\begin{aligned} 2\mathrm{H_2O} &\Leftrightarrow 2\mathrm{H}^{+} + 2(\mathrm{OH})^{-}, \\ \mathrm{As}^{3+} + 2(\mathrm{OH})^{-} &\rightarrow \mathrm{AsO_2^{-}} + 2\mathrm{H}^{+}, \\ 2\mathrm{AsO_2^{-}} + 2\mathrm{H}^{+} &\rightarrow \mathrm{As_2O_3} + \mathrm{H_2O}; \end{aligned} \tag{3}$$

finally the overall reaction is

$$\begin{aligned} 2\mathrm{GaAs} + 12^{+} + 10\mathrm{H_2O} \\ \rightarrow \mathrm{Ga_2O_3} + \mathrm{As_2O_3} + 4\mathrm{H_2O} + 12\mathrm{H}^{+}. \end{aligned} \tag{4}$$

The gallium and the arsenic oxides are dissolved in acids or bases, that form part of the etchant solution, and thus the etching is completed [33].

The reaction for the reductive decomposition of p-GaAs is suggested to be

$$\mathrm{GaAs} + 6e^{-} \rightarrow \mathrm{Ga} + \mathrm{As}^{3-} \tag{5}$$

and the overall reaction in presence of water becomes

$$\begin{aligned} 2\mathrm{GaAs} + 6e^{+} + 6\mathrm{H_2O} \\ \rightarrow 2\mathrm{Ga} + \mathrm{As_2O_3} + 3\mathrm{H_2O} + 6\mathrm{H}^{+}. \end{aligned} \tag{6}$$

In this case the process has the complication that the more stable Ga remains on the surface forming a layer and inhibiting the etching process. This means, from an experimental point of view, it is simpler to etch n-type GaAs than p-type. However a method has been reported to easily etch p-type material. By using an external potential it is possible to increase the surface hole concentration to oxidize and then dissolve the Ga more rapidly [34]. Such method still has the inconvenience of adding more parameters to the analysis and more components to the experimental set-up, which complicates the process itself.

When processing a semiconductor by photoetching, is important to keep in mind the type of dopant in the material. This property has been used for selectively etching different sections in a GaAs homostructure substrate [35].

Most common liquid etchants for GaAs LACE are $H_2SO_4/H_2O_2/H_2O$ in proportion 1/1/100 by volume, HNO_3/H_2O in proportion 1/20 or 1/10 by volume, and KOH/H_2O in 1/20 by weight; while Cl_2 and CCl_4 stand among the most used gaseous etchants [36, 37]. For a more detailed study of the laser assisted chemical process, the reader is referred to some additional literature on this subject [38, 39].

Concerning to the SHUR processing, the photoetch procedure starts after the sample has been removed from the MOCVD reactor after the first growth step (Fig. 3). Following a typical sample cleaning routine, LACE was performed on the GaAs layer using an Ar^{+} laser ($\lambda = 488$ nm) and a HNO_3/H_2O:1/10 (by volume) etching solution, that was chosen to allow a good etch control. During the chemical reaction the $(OH)^{-}$ radical in the water acts as the oxidizing agent while nitric acid dissolves Ga and As oxides.

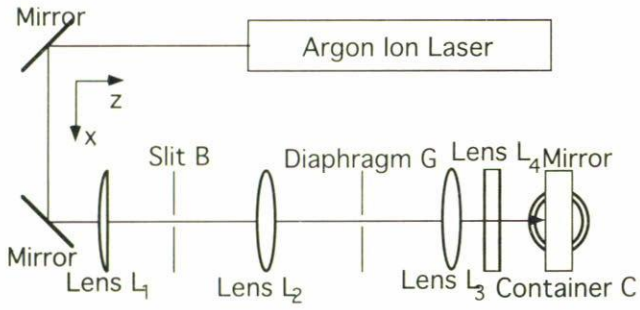

FIGURE 9. Top view diagram of whole optical system set up, used for laser assisted etching experiments.

Appendix B. Optical system for LACE

The optical set-up is shown in Fig. 9, where L_1 is a plane-convex cylindrical lens of focal length 21 cm used to focus the laser beam in the lateral direction to fill the slit B (whose adjustable aperture can be changed to vary the width of the etching profile) and L_2 is a positive lens with a focal length of 21 cm to form the Fourier transform of the slit B. At an approximate focal length distance to the right side of L_2, an aperture G filters the side lobes but propagates the central lobe of the sinc^2 slit pattern. Intermediate L_3 is another positive lens similar to L_2 that is located two focal lengths from the aperture G and forms the image of the central lobe of the sinc^2 directly on the sample. (This was done by first forming an image of the aperture G directly on the substrate, using incoherent illumination.)

Subsequent L_4 is a plane-concave cylindrical lens used to stretch the final image in the vertical direction and finally the container C, that holds the material sample and the etchant chemicals, is located two focal lengths behind lens L_3. This optical system creates, at the etching plane, an approximately quadratic intensity variation beam in the lateral x-direction along a line of about 1 cm length. (Alternative optical arrangements are also possible that achieve the same purpose.)

The container C was a 100 cc cylindrical glass beaker. The sample was laying horizontally on a Teflon cube 2 cm per side. The container holding the sample was fixed on top of an stepper used for multiexposure purposes, programmed to step 400 μm between each exposure.

A relation between the slit's width and the spatial filter aperture can be established as follows. In Fig. 10, it is assumed that the slit B is uniformly illuminated by a laser beam. If the width of this slit is b, hence its transmittance function at the x-axis becomes

$$f(x) = \begin{cases} 1, & \text{if} |x| \leq \dfrac{b}{2} \\ 0, & \text{elsewhere} \end{cases} \tag{7}$$

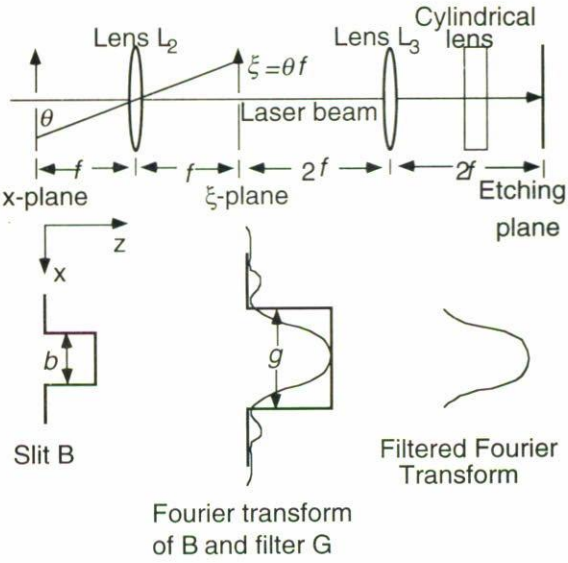

FIGURE 10. Analysis of the optical set-up section that performs the beam filtering for laser assisted etching.

At a focal distance f behind lens L_2, at plane ξ, (on filter G) the light intensity distribution can be shown to be the well known sinc^2 function:

$$I = I_0 \left(\frac{\sin \beta}{\beta} \right)^2, \tag{8}$$

with I_0 being the maximum intensity, likewise

$$\beta = \frac{kb\theta}{2}, \quad \text{and} \quad k = \frac{2\pi}{\lambda}, \tag{9}$$

where k is the wave number.

In the paraxial approximation, one can say that

$$\xi = \theta f. \tag{10}$$

The first minimum of function in Eq. (8) corresponds to

$$\beta = \pi \tag{11}$$

Substituting Eq. (11) in Eq. (9) and combining with Eq. (10), the size g of the spatial filtering slit needed to pass only the central lobe of the sinc^2 pattern results

$$g = \frac{2f\lambda}{b}. \tag{12}$$

So, the filter width g depends on the focal length of the lens L_2, the wavelength λ of the laser and the size of the slit b. Hence several possibilities exist to select the desired g filter width. The lens L_3 forms the image of the central lobe directly on the sample and the cylindrical lens stretches the image in y-direction.

1. R.M. Osgood and H.H. Gilgen, *Ann. Rev. Mater. Sci.* **15** (1985) 549.
2. J.G. Eden, "Photochemical Processing of Semiconductors: New Applications for Visible and Ultraviolet Lasers," *IEEE Circuits and Devices Magazine*, January, 1986).
3. M.S. Allen, S. Guel-Sandoval, and J.G. McInerney, *Proc. of SPIE* **1634** (1992) 420.
4. A.E. Siegman, *Lasers*, Chaps. 19 and 22, (University Science Books, Mill Valley CA, 1986).
5. A.E. Siegman, *Appl. Opt.* **13** (1974) 353.
6. H. Kogelnik and T. Li, *Proc. of the IEEE* **54** (1966) 1312.
7. D.R. Scifres, R.D. Burnham, and W. Streifer, *Appl. Phys. Lett.* **33** (1978) 1015.
8. D.E. Ackley and R.W.H. Engelmann, *Appl. Phys. Lett.* **39** (1981) 27.
9. D. Botez *et al.*, *Appl. Phys. Lett.* **53** (1988) 464.
10. D. Mehuys, J. Major Jr., and D.F. Welch, *Proc. of SPIE* **1850** (1993) 2.
11. A.A. Golubentsev, V.V. Likhanskii, and A.P. Napartovich, *Sov. Phys. JETP* **66** (1987) 676.
12. C. Roychoudhuri *et al.*, *LEOS '88 Annual Meeting Proc.* Paper FE.4 (1988) 477.
13. L.J. Mawst *et al.*, *Electron. Lett.* **25** (1989) 365.
14. D. Mehuys, D.F. Welch, and L. Goldberg, *Electron. Lett.* **28** (1992) 1944.
15. R. Parke *et al.*, *IEEE Phot. Tech. Lett.* **5** (1993) 297.
16. A.P. Bogatov *et al.*, *Sov. J. Quantum Electron.* **10** (1980) 620.
17. R.R. Craig *et al.*, *Electron. Lett.* **21** (1985) 62.
18. J. Salzman *et al.*, *Appl. Phys. Lett.* **46** (1985) 218.
19. C. Largent *et al.*, *Proc. of SPIE* **1418** (1991) 40.
20. M.L. Tilton *et al.*, *IEEE J. Quantum Electron.* **27** (1991) 2098.
21. R.K. DeFreez *et al.*, *Proc. of SPIE* **1850** (1993) 75.
22. S.T. Srinivasan *et al.*, *Appl. Phys. Lett.* **61** (1992) 1272.
23. S. Guel-Sandoval *et al.*, *Appl. Phys. Lett.* **66** (1995) 2048.
24. A.H. Paxton, C.F. Schaus, and S.T. Srinivasan, *IEEE J. Quantum Electron.* **29** (1993) 2784.
25. J.W. Goodman, *Introduction to Fourier Optics*, McGraw-Hill, New York, (1968), Chaps. 5 and 7.
26. R.M. Osgood Jr. *et al.*, *Appl. Phys. Lett.* **40** (1982) 391.
27. G.C. Tisone and A.W. Johnson, *Appl. Phys. Lett.* **42** (1983) 530.
28. S. Guel-Sandoval, A.H. Paxton, S.D. Hersee, and J.G. McInerney, *Rev. Mex. Fís.* **43** (1997) 940.
29. D.V. Podlesnik *et al.*, *J. Opt. Soc. Am. B* **3** (1986) 775.
30. R.M. Osgood Jr., A. Sanchez-Rubio, D.J. Ehrlich, and V. Daneu, *Appl. Phys. Lett.* **40** (1982) 391.
31. A.E. Willner *et al.*, *Proc. of SPIE* **946** (1988) 48.
32. G.C. Tisone, and A.W. Johnson, *Appl. Phys. Lett.* **42** (1983) 530.
33. S.K. Ghandhi, *VLSI Fabrication Principles Silicon and Gallium Arsenide*, (Wiley and Sons, New York, 1983), Chaps. 7 and 9.
34. F.W. Ostermayer Jr. and P.A. Kohl, *Appl. Phys. Lett.* **39** (1981) 76.
35. R. Khare and E.L. Hu, *J. Electrochem. Soc.* **138** (1991) 1516.
36. D.V. Podlesnik, H.H. Gilgen, A.E. Willner, and R.M. Osgood Jr., *J. Opt. Soc. Am. B* **3** (1986) 775.
37. M. Takai *et al.*, *Mat. Res. Soc. Symp. Proc.* **29** (1884) 211.
38. F.A. Houle, *Appl. Phys. A* **41** (1986) 315.
39. D.V. Podlesnik and H.H. Gilgen, in *Laser chemical processing for microelectronics*, (Cambridge University Press, New York, 1989), Chap . 4.